Article

Simulation on Secondary Electron Multiplication Behavior of the Microchannel Plate under DC Mode

Fengyan Li [1], Dongyu Jiang [1,2], Peng Jiao [2], Yong Sun [2] and Yonggang Huang [2,*]

[1] School of Textiles and Engineering, Tiangong University, Tianjin 300386, China
[2] Institute of Special Glass Fiber and Optoelectronic Functional Materials, China Building Materials Academy, Beijing 100024, China
* Correspondence: huangyonggang@cbma.com.cn

Abstract: In this study, a three-dimensional microchannel model of a single hollow-core glass fiber was constructed and the Finite Integral Technique and Monte Carlo method were combined to comprehensively simulate the electron multiplication process in a single channel under DC mode. The electron dynamic trajectory in DC electron emission mode was achieved. The effects of different structural parameters and applied bias voltage on the electron gain and the most probable exit energy at the output end of MCP were investigated. The results show that the electrons with a certain initial current can be continuously and stably multiplied in the channel under DC mode and eventually reach a stable value because of the space charge effect; additionally, the electron gain increases with the increase in the bias angle and DC bias voltage and decreases with the increase in the penetration depth of the MCP output electrode. The electron gain at the output end of the MCP increases with the length-to-diameter ratio under the normalized voltage but shows a maximum value under the constant voltage. The simulation results are consistent with the reported experimental trend and theoretical analyses. The method provides data support for the optimal structural design of the microchannel plate.

Keywords: microchannel plate; secondary electron; DC mode; electron multiplication; theoretical simulation

1. Introduction

Micro-channel Plate (MCP) is a beehive-like array comprising tens or even hundreds of millions of hollow-core glass fiber that play role of electron multipliers and can achieve an "avalanche" multiplication of electron or photoelectron flow. It is the core component of devices such as image intensifier tubes, space ray detection imaging, and electron detection and counting and is widely used in many fields including low light night vision, nuclear diagnostics, space science, and analytical instruments [1–5].

The secondary electron multiplication is the key property of microchannel plates, which directly determines the spatial resolution, temporal resolution, intensity and quantity detection, and identification of weak photoelectron signals. The secondary electron emitted from the surface of each hollow-core glass fiber in the microchannel plate is the basis for its electron multiplication. It is related to the composition and structure of the micropore surface [6]. Some studies [7–9] experimentally obtained the effect trend of microchannel plate preparation parameters on the electron multiplication of MCP. These parameters include acid etching to form micropores, hydrogen reduction to form semiconductor layers, output–electrode penetration depth, and bias angle variation. Meanwhile, the mechanism of secondary electron multiplication in the channel was theoretically elucidated and an ideal structural model of the microchannel plate surface was proposed. However, due to the complicated and costly fabrication process of MCP, there are many factors influencing electron multiplication performance. Furthermore, the micropores are small in scale and curved in shape. All these lead to the difficulties for experimental studies and measures.

The current experimental studies are limited to the macroscopic behavior of MCP. There are few systematic investigations on the multiplication behavior of electrons in the channel from a microscopic perspective. As a result, the agreement between theoretical and experimental results has not been very well investigated. The construction of theoretical modeling and simulation on secondary electron multiplication behavior, therefore, plays an important role in studying the microscopic and dynamic multiplication behavior of secondary electrons. Based on the simulations, important parameters such as transit time, collision energy and angle, multiplication number, direction, and energy can be obtained to describe the transport process of multiplication electrons. Furthermore, the multiplication performance of secondary electrons is expected to be explained clearly.

Regarding the popular electron multiplication theory, i.e., energy proportionality assumption, of the microchannel plate [9], Chang simulated the selectivity of the microchannel plate under Gaussian pulse voltage and considered that the exposure time could be reduced by the reduction in electrical pulse width and increase in electrical pulse amplitude and the gain of the microchannel plate was consequently increased [10]. Cai et al. [11] reported the selectivity of the MCP with different selectivity pulse waveforms when injecting a Gaussian pulse electron at the input surface of the microchannel plate and considered that the trapezoidal waveform was optimal. Furthermore, Cai et al. [12,13] investigated the effect of the DC bias voltage applied to both ends of the microchannel plate on the spatial resolution, the mean value of the angular distribution of the electrons at the output end of the MCP, and the FWHM of the angular distribution using the Monte Carlo method. Deng et al. [14] verified that the selective pulse transmission attenuation affects the gain of the microchannel plate when it is applied in microstrip lines. Using a Gaussian pulse mode to emit electrons at the input surface, Chen et al. simulated the MCP using CST Studio Suite simulation software and combined it with the Finite Integral Technique (FIT) and Monte Carlo random distribution model to analyze the effect of DC bias voltage on gain and electron transit time [15]. Yang et al. [16] varied the V_{MCP1}, V_{MCP2}, and V_{gap} of a two-chip microchannel plate in a Chevron configuration to study the MCP gain performance and single-electron resolution under different plate biases. Still, there are some examples in the literature [17,18] to calculate gain, transit time, and other parameters of MCP under DC bias and pulse bias voltage, by their self-developed Monte Carlo program, respectively. For the above-mentioned simulations, the emission mode of electrons is focused on the Gaussian pulse and the variation of Gaussian pulse parameters has a significant effect on the results.

In the practical applications of MCP, besides the reported pulsed emission of electrons, a DC mode, i.e., a continuous operation mode, is also one of the important signal sources inside the incident MCP micropores [19]. However, according to our knowledge, the study of the secondary electron multiplication behavior under the DC mode has not yet been reported using three-dimensional numerical simulations. In this study, the secondary electron multiplication process in a microchannel plate under DC electron emission mode was simulated by a commercial finite element simulation software. Based on the Finite Integral Technique (FIT) and Monte Carlo random distribution model, the influence of output–electrode penetration depth, the length-to-diameter ratio, the bias angle, and the applied voltage at both electrode surfaces of the channel on the electron multiplication behavior was microscopically obtained. The simulation results will provide theoretical support for improving the electron gain of the microchannel plates and also be a method to verify the agreement between the electron multiplication theory of microchannel plates and experimental data operating in DC mode.

2. Theoretical Model for Simulation

2.1. Construction of a 3D Single Channel Model

As shown in Figure 1a, there are millions of uniform hollow-core glass tubes in the MCP. The incident electrons are multiplied during each hollow-core glass tube (Figure 1b) until they are transported from the output end and then converted into photons on the

fluorescent screen to form a clear image. To improve the efficiency of the theoretical simulation, a three-dimensional microchannel model of a single hollow-core glass fiber was constructed. The electron generating devices and electron collecting devices were set at the input and output electrode surface of the microchannel, as shown in Figure 1c. In the figure: l_1 is the input–electrode penetration depth, l_2 is the output–electrode penetration depth, L is the channel length, D is the channel inner diameter, and θ is the channel bias angle.
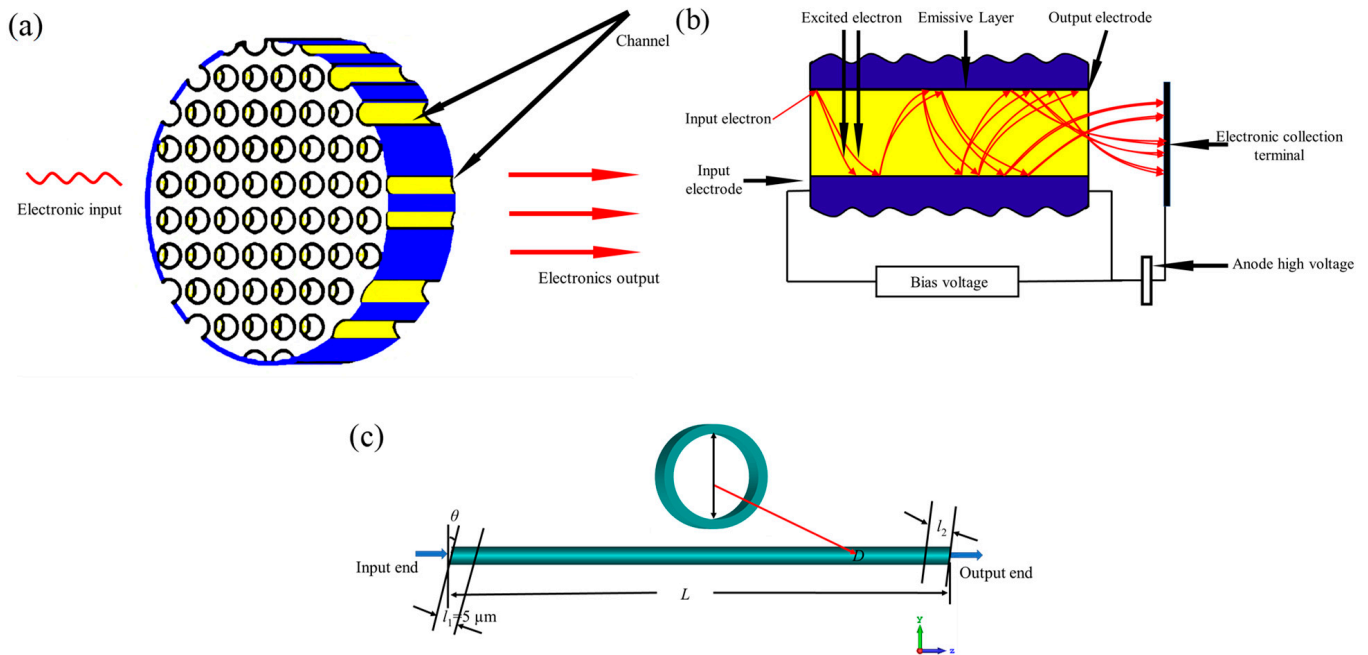

Figure 1. MCP multiplication process and model construction: (**a**) Microchannel plate structure; (**b**) Single channel electron multiplication principle; (**c**) 3D single channel model.

In the simulation, the aperture diameter of the single channel is 10 μm, the channel material is selected as lead glass with a dielectric constant of 6, and the electrode material at both ends is set as an ideal electrical conductor (PEC). One electron is introduced at the input end of the microchannel plate and incident perpendicular to the surface into the channel with an input current density of 1.0×10^{-11} A/m^2 and initial energy of 300 eV.

2.2. Simulation of Secondary Electron Multiplication Behavior in Microchannels

2.2.1. Theoretical Model of Electron Multiplication

The most representative theoretical models of electron gain in microchannel plates are the energy-proportional assumption model [9] and the Furman model [20]. Among them, the Furman model corrects the problem of consistent behavior of all electrons collision and reflects electron collisions more realistically; the Monte Carlo random model expresses the true secondary electron yield as a Poisson distribution and the secondary emission angle obeying a ~cos θ distribution, completely independent of the primary incident angle and incident energy; considering the energy conservation of emitted electrons, the total energy of secondary electrons, including true secondary electrons, backscattered electrons, and diffused electrons, does not exceed the primary electron energy. Moreover, the energy of any given secondary electrons is lower than the primary electron energy. Figure 2 shows the secondary electron energy distribution for a primary electron of 100 eV. The true secondary electrons located in the low-energy region are a major part of the total secondary electrons, whose energy is usually only a few electron volts, lower than that of the backscattered electrons.
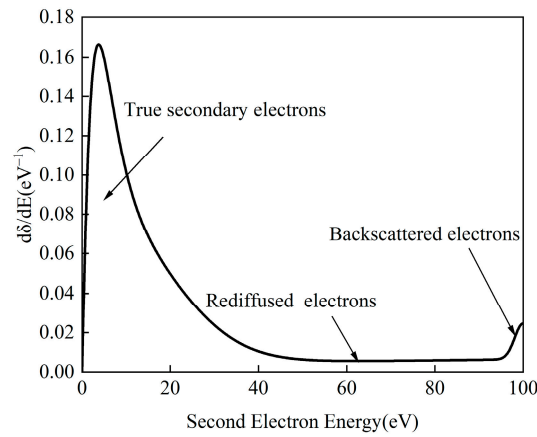
Figure 2. Secondary electron energy distribution.

In this simulation, the secondary emission probability model proposed by Furman et al. is used, which contains three types of secondary electrons, i.e., backscattered secondary electrons, rediffused secondary electrons, and true secondary electrons. The electron yield and the setting values are employed in our simulation [21].

The backscattered electrons:

$$\delta_{\rm bs}(E,0) = P_{1,\ \rm bs}(\infty) + \left(\hat{P}_{1,\rm bs} - P_{1,\rm bs}(\infty)\right) \times {\rm e}^{-\left(\frac{|E-\hat{E}_{\rm bs}|}{W_{\rm bs}}\right)^{P}/P};\ \delta_{\rm bs}(E,\theta) = \delta_{\rm bs}(E,0)[1 + e_1(1 - \cos^{e_2}\theta)]$$

$$(\delta_{\rm bs})_{\rm max} = 0.05,\ E = 0.0,\ P_1 = 0.05,\ W = 100,\ P = 0.9,\ e_1 = 0.26,\ e_2 = 2.0.$$

The rediffused secondary electron:

$$\delta_{\rm rd}(E,0) = P_{1,\rm rd}(\infty)\left[1 - e^{-\left(\frac{E}{E_{\rm rd}}\right)^{r}}\right];\ \delta_{\rm rd}(E,\theta) = \delta_{\rm rd}(E,0)[1 + r_1(1 - \cos^{r_2}\theta)]$$

$$(\delta_{\rm rd})_{\rm max} = 0.5,\ E = 40.0\ {\rm eV},\ P_1 = 0.5,\ r = 1.0,\ r_1 = 0.26,\ r_2 = 2.0.$$

The true secondary electron yield:

$$\delta_{\rm ts}(E,\theta) = \hat{\delta}(\theta)D\left(\frac{E}{\hat{E}(\theta)}\right);\ D(x) = \frac{sx}{s-1+x^s}$$

$$\hat{\delta}(\theta) = \hat{\delta}_{\rm ts}\left[1 + t_1\left(1 - \cos^{t_2}\theta\right)\right];\ \hat{E}(\theta) = \hat{E_{\rm ts}}\left[1 + t_3\left(\hat{1} - \cos^{t_4}\theta\right)\right]$$

$$(\delta_{\rm ts})_{\rm max} = 3.46,\ E = 260\ {\rm eV},\ s = 1.813,\ t_1 = 0.66,\ t_2 = 0.80,\ t_3 = 0.70,\ t_4 = 1.00.$$

where $\delta_{\rm bs}(E, 0)$ and $\delta_{\rm rd}(E, 0)$ are the values of $\delta_{\rm bs}(E, \theta)$ and $\delta_{\rm rd}(E, \theta)$ at the perpendicular incidence of electrons ($\theta = 0$). $P_{1,\rm bs}(\infty)$ and $P_{1,\rm rd}(\infty)$ are the probability $P_{1,\rm bs}$ and $P_{1,\rm rd}$ at the perpendicular incidence of electrons of infinite energy. $\hat{P}_{1,\rm bs}$ and $\hat{\delta}_{\rm ts}$ are the peak values at the maximum energy $\hat{E}_{\rm bs}$ and $\hat{E}_{\rm ts}$. E and θ are the primary incidence energy and angle. $D(x)$ is a scaling function. $W_{\rm bs}$, P, $E_{\rm rd}$, and r are fitting parameters. e_1, e_2, r_1, r_2, and s are adjustable parameters.

2.2.2. Theoretical Simulation Solver

The PIC algorithm is a self-consistent simulation method for electron tracking. The incident electrons in the microchannel are accelerated by the electric field and then the movement of a large number of electrons interferes with the distribution of the channel electrostatic field. The PIC algorithm considers the influences of the internal electric field and the space charge field generated by charged secondary electrons on the electrons. The electric field will be updated with time. Then, the electric field, electron trajectory, energy, and velocity are calculated [22]. Therefore, the PIC solver is selected to calculate the electric

field and the electron variation with time in discrete time, the field at discrete positions, and to track the electron state at continuous phase space positions.

3. Simulation Results and Discussion

3.1. Electric Field Distribution in the Channel

Each hollow glass fiber in MCP can be regarded as a cylindrical glass tube. The inner surface of the tube has a semiconductor layer with secondary emission characteristics and both electrode surfaces of the channel are coated with electrodes. The material of the channel in this study is lead glass with a conductivity of 1.0×10^{-7} S/m. The secondary electron emission coefficient of the inner wall of the channel is 3.46 and the energy of primary electrons incident vertically to the surface is 260 eV. The electrodes at the ends of the channel are ideal conductors (PEC) with a secondary electron emission coefficient of 1 and the energy of primary electrons incident vertically to the surface is 500 eV. When the voltage is applied between the two electrodes, a uniformly distributed axial electric field is generated in the channel, as shown in Figure 3.
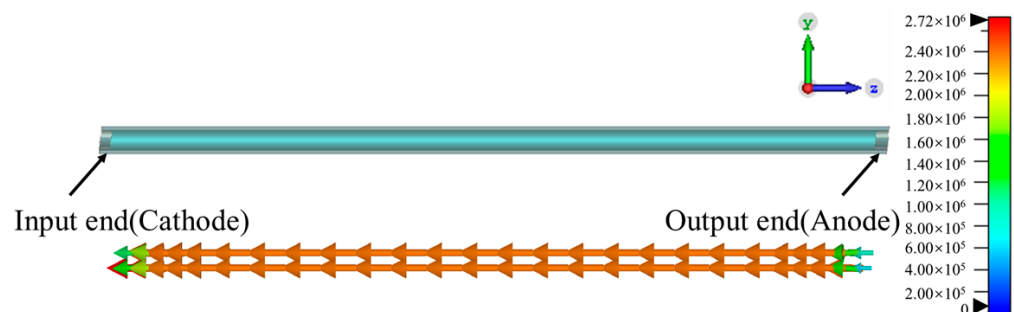

Figure 3. Electric field distribution inside MCP hollow-core glass fiber.

When primary electrons are incident from the input surface of the channel and collide with the inner wall, secondary electrons are generated. Secondary electrons with a lower initial transverse velocity component enter the axial electric field and move along the channel in a parabolic trajectory under the uniform electric field until they collide with the channel wall again, generating more secondary electrons.

3.2. Simulation of Electron Multiplication Process in the Channel

3.2.1. Electron Motion Trajectory

Setting a monitor at the output end of the MCP as shown in Figure 1c, the 3D trajectory of electrons at different transit times were illustrated in Figure 4. With the increase in the transition time, the number of electrons in the channel under DC emission mode increases cumulatively along the length direction, which is caused by more secondary electrons escaping from the inner wall of the channel after the collision of the incident electrons. A small number of secondary electrons reach the output end of the MCP and escape out of the channel from the transition time of 70 ps. Thereafter, as the transition time increases, more and more electrons are exported. In the DC emission mode, the current continuously provides input electrons with the initial current density and the electrons continuously collide with the inner wall of the channel. More and more electrons will be accumulated in the channel and transported to the exit end of the MCP. At 70 ps, the electrons in DC mode start to come out from the output end of the MCP until saturation at the electrode surfaces of the channel. This is completely different from the trajectory of electrons under Gaussian pulses [11].
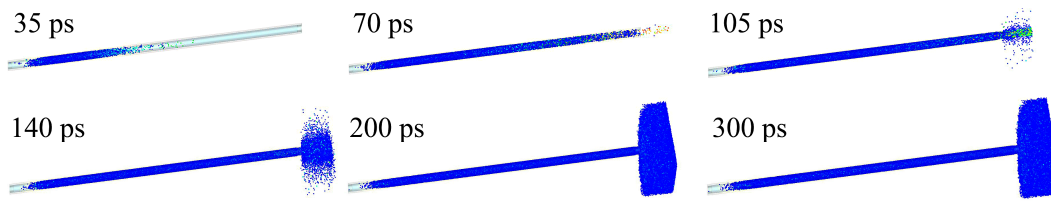
Figure 4. The trajectory of electron motion in the channel under the DC mode.

3.2.2. Electron Multiplication at Different Transit Times

The gain and the distribution of the most probable exit energy at the output end of the MCP are counted at different transit times and the results were shown in Figure 5. The electronic gain of the microchannel plate is calculated by $G = I_1/I_0$ (I_1 is current density of the output end. I_0 is current density of the input electrons, 1.0×10^{-11} A/m^2).
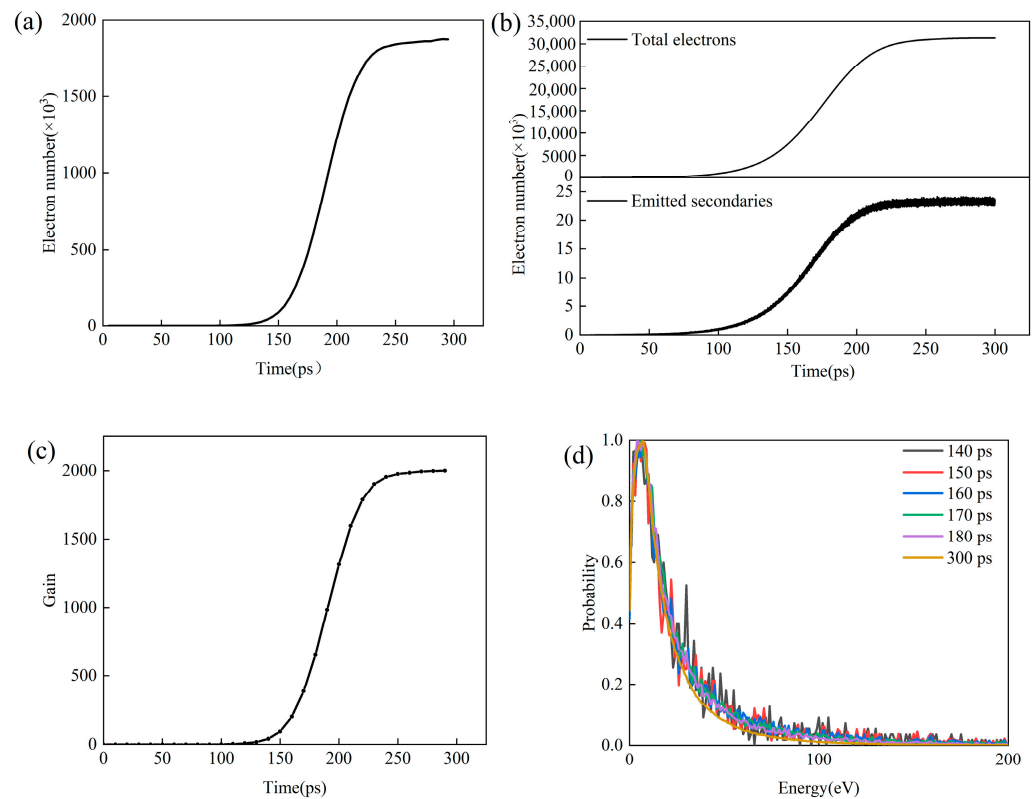

Figure 5. Simulation results of electron multiplication behavior of MCP with different transit times: (**a**) Accumulative electronic number at the output end; (**b**) Accumulative electronic number in the channel; (**c**) Gain; (**d**) The most probable exit energy distribution.

As seen in Figure 5, the number of electrons in the channel gradually increases with the transit time. In the DC emission mode, an incident electron reaches the set steady-state current density (1.0×10^{-11} A/m^2) after 0.1 ps, i.e., the emission current. Then, the electrons collide with the inner wall under the uniform electric field produced by the added bias voltage at both ends of the channel. The velocity and displacement of the electron motion are computed based on the charged electron equation and then the new collisions of electrons with the inner wall occur. Such a process continues resulting in the continuous emission of secondary electrons from the inner wall of the channel. Therefore, the number of electrons in the channel is increasing. Consequently, the number of electrons escaping from the output end of the MCP increases. The electron gain rises significantly from 130 ps to 190 ps. As the number of particles in the channel continues to increase, the gain shows a slow increase from 190 ps (see Figure 5c). The PIC solver used for simulations takes into

account the effect of the space charge of the electron. Due to the increasing amount of accumulated charge at the output end of the MCP, the formed space charge field is opposite to the DC bias field within the single channel and the two fields superimpose on each other, forming a space charge saturation effect [23], which in turn leads to a gradual decrease in the electric field, a saturation of the current density, and a decrease in the rate of gain rise, reaching saturation at the output end of the MCP. Figure 5d shows the most probable exit energy distribution of the secondary electrons at the output end of the MCP at different transit times. It is seen that the energy distribution trend is the same, with the final particles at the output end of the MCP having the most concentrated energy at 7 eV.

3.3. Influence of Structural Parameters on Electron Multiplication

3.3.1. Penetration Depth of MCP Output Electrode

Varying the electrode depth at the output end of the microchannel, the electric field intensity in the channel was shown in Figure 6. The voltage applied at both ends of the channel is 900 V, the length-to-diameter ratio is 39, and the bias angle is 6°. The inset of the figure shows the effect of the output–electrode penetration depth on the electric field intensity in the channel at 200 μm along the channel length. According to the literature [24,25], the electric field inside the channel can be divided into two parts, the constant–potential region generated by the coated electrode portion at both ends and the high-field region in the middle of the channel. In the high-field region, the field intensity inside the channel increases with the increase in the output–electrode penetration depth. In the constant–potential region as seen in the enlarged figure, the coated electrode material is an ideal electrical conductor (PEC), the potential in the electrode region is constant, and the field intensity is zero. The greater the output–electrode penetration depth vaporized at the output electrode surface, the earlier the decreasing in the electric field intensity. Additionally, then a wider range of the constant–potential region at the output end of the MCP is formed.
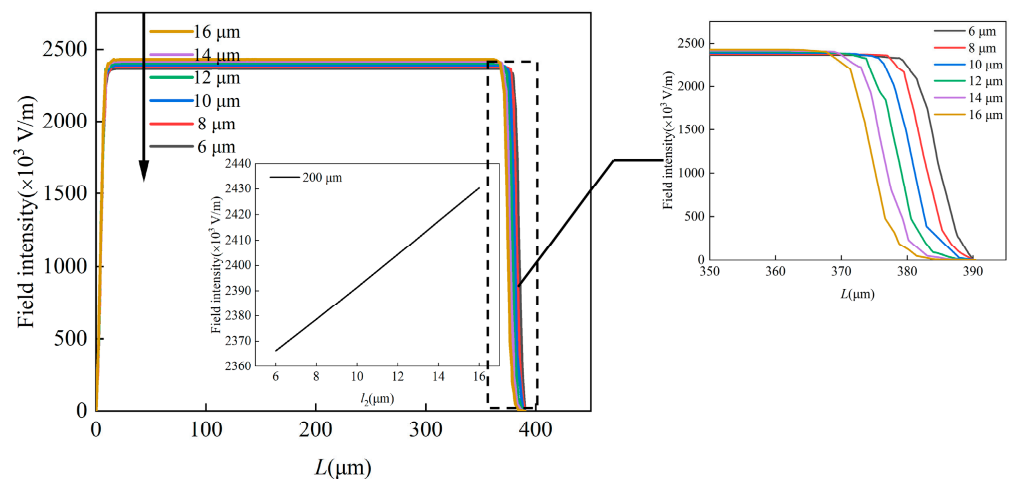

Figure 6. Effect of the penetration depth on the field intensity in the channel.

The influence of output–electrode penetration depth on the secondary electron multiplication at a DC mode were shown in Figure 7. The electrode at the output end of the microchannel plate is the anode and the electrode absorbs some electrons when the electrons move to the end, i.e., electrode end spoiling, which directly affects the electron gain. The greater the output–electrode penetration depth, the more absorbed electrons there are. From Figures 6 and 7a, it can be concluded that the gains are affected by the electric field intensity and the output–electrode penetration depth simultaneously. The gain decreases gradually with the increase in the output–electrode penetration depth, showing the significant influence of the output–electrode penetration depth on gain. With the increasing of l_2 from 6 μm to 16 μm, the increased electric field in the high-field region

excite more electrons from the inner surface of the channel. On the contrary, these electrons will be absorbed with the greatest probabilities when transported along the channel to the anode. It is evidenced that the gain is the smallest at the output–electron penetration depth of 16 μm. The most probable exit energy and FWHM at 16 μm are the lowest. It indicates the increase in the number of secondary electrons output from MCP. Our simulated results are in accordance with Chen et al. [26].
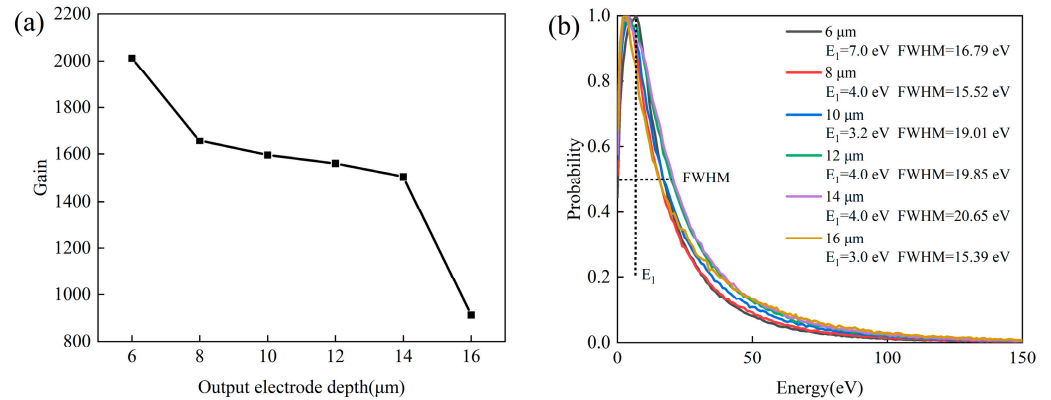

Figure 7. Effect of output–electrode penetration depth on secondary electron multiplication (bias voltage = 900 V, L/D = 39, θ = 6°): (**a**) Gain; (**b**) The most probable exit energy distribution.

3.3.2. Bias Angle

Fixing the voltage applied at both ends of the channel to 900 V, the length-to-diameter ratio is 39 and the output–electrode penetration depth is 16 μm, the variation of secondary electron multiplication with bias angle at a DC mode was simulated and shown in Figure 8.
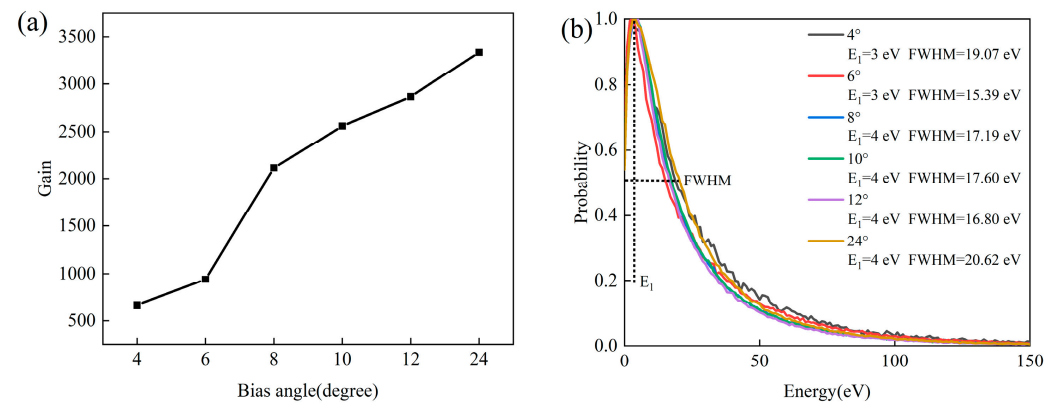

Figure 8. Effect of the bias angle on secondary electron multiplication (bias voltage = 900 V, L/D = 39, l_2 = 16 μm): (**a**) Gain; (**b**) The most probable exit energy distribution.

When the bias angle increases from 4° to 24°, the gain gradually increases from 662 to 3338 and the most probable exit energies at the output end of the MCP are around 4 eV. According to Rochau et al. [27], the steady-state gain (G) of the electrons is well approximated by Equations (1) and (2). The larger bias angle decreases the electron birth depth and then the gain increases. This is due to the increases in the numbers of electron collision on the inner surface of MCP. Both the most probable exit energy and the FWHM is the smallest at the bias angle of 6°, indicating the concentrated energy.

$$G(\theta) = \left(\frac{V}{V_0}\right)^{L/4D\left(1 - x_n(\theta)/L\right)} \tag{1}$$

$$x_n(\theta) = d \cot \theta \tag{2}$$

where V is bias voltage applied at two ends of the channel, V_0 is turn-on voltage dependent upon material properties, L/D is length-to-diameter ratio, θ is incident angle of primary electrons which is proportional to bias angle, and x_n is electron birth depth.

3.3.3. Length-to-Diameter Ratio

With a fixed channel inner diameter of 10 μm, the output–electrode penetration depth of 6 μm, and bias angle of 6°, changing the length-to-diameter ratio (L/D), the secondary electron multiplication behavior at a DC mode was simulated and analyzed and the results operated at a normalized voltage were shown in Figure 9.
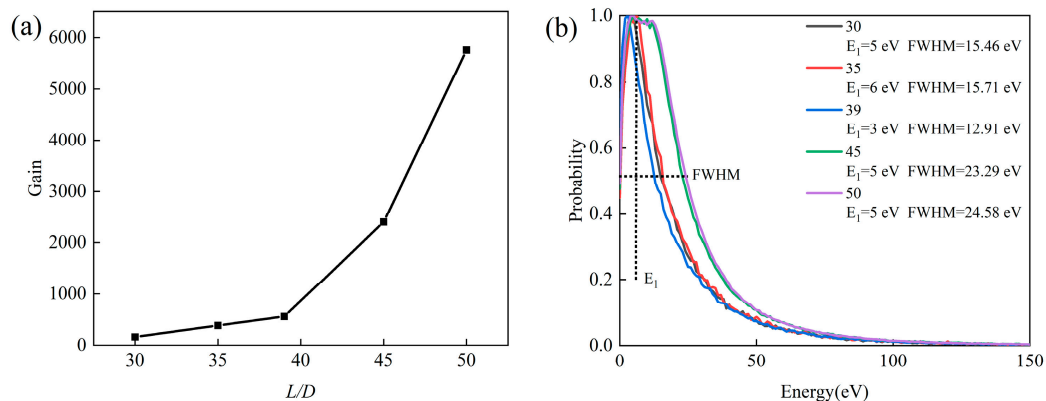

Figure 9. Effect of L/D on secondary electron multiplication at the normalized voltage ($\theta = 6°$, $l_2 = 6$ μm): (**a**) Gain; (**b**) The most probable exit energy distribution.

The normalized voltage is calculated by $W = U/\alpha$, where U is the operating voltage, α is L/D of the MCP. For a specific operating voltage, there exists an optimal value α corresponding to the maximum gain. Based on the practical tests, the optimal operating voltage to the optimal length-to-diameter ratio for microchannel plates is usually $U = 22\alpha$ [15]. The normalized voltage is kept constant and the length-to-diameter ratio of the microchannel plate is measured as 30, 35, 39, 45, and 50, respectively. The simulated results show that the gain increases significantly with the increase in the length-to-diameter ratio. Obviously, the gain is the maximum value for each L/D due to the normalized voltages. In this case, it can be concluded that the long L/D elongate the distance that the electrons collide with the inner surface of MCP. This results in the increasing number of emitted secondary electrons. Figure 9b shows the most probable exit energy distribution at the output end of the MCP under different L/D. Obviously, when the L/D is 39, the electron energy distribution at the output end of the MCP is the most concentrated, which causes it to be easy to gather electron optics and facilitates better spatial resolution. The L/D of the MCP will have a great influence on its gain, but, at the same time, the thickness should be considered. Under certain applied voltage conditions, being too thin will affect the mechanical properties of the microchannel plate and increase the manufacturing difficulty, so it is necessary to select the optimum gain by balancing the manufacturing difficulty and applied bias voltage at the same time.

According to the test results of the optimal L/D at the normalized voltage, keeping the channel inner diameter (10 μm), the output–electrode penetration depth (6 μm) and the channel voltage (850 V) are constant and the influence of L/D on the secondary electron multiplication was further simulated and shown in Figure 10; this illustrates a maximum gain at $L/D = 20$. This is attributed with the variation of electric field strength and electron cascade generation with L/D. Under current simulation conditions, if L/D is higher than 20, the increase in the L/D, i.e., the increase in the channel length, causes the electric field strength at both ends of the channel to decrease, which in turn reduces the impact energy of the electrons. The low-energy electrons reduce the number of impacts in the channel, resulting in a lower secondary electron yield and a lower gain of the microchannel plate. Lower than 20, a too short channel length is not enough to generate more electron cascades; this will cause low gain. This is in agreement with the previous study [15]. From the most

probable exit energy distribution in Figure 10b, the most probable exit energy value of the electrons at the output end of the MCP reaches the lowest value at the length-to-diameter ratio of 39, i.e., the most concentrated energy distribution.
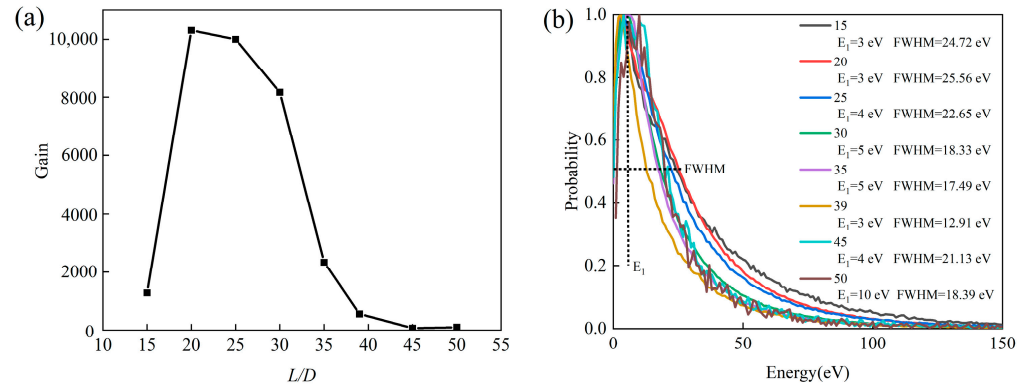

Figure 10. Effect of L/D on secondary electron multiplication at the same applied voltage (bias voltage = 850 V, $\theta = 6°$, $l_2 = 6$ μm): (**a**) Gain; (**b**) The most probable exit energy distribution.

3.4. Influence of Bias Voltage on Electron Multiplication

With a fixed output–electrode penetration depth of 6 μm, the length-to-diameter ratio of 39, and the bias angle of 6°, the electric field intensity in the channel varies by varying the applied bias voltage from 700 V to 1000 V at the two ends of the channel. The result was shown in Figure 11. The inset shows the effect of the applied voltage at both ends of the channel on the electric field intensity at the channel length of 200 μm.
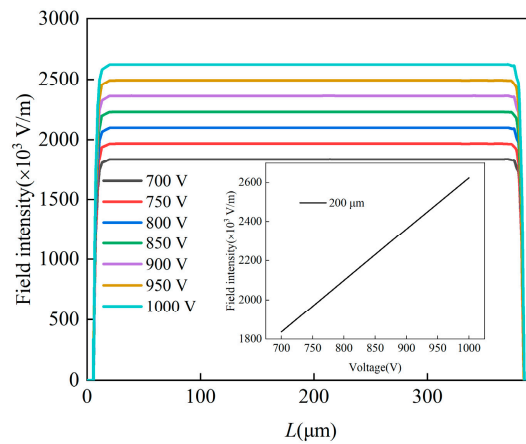

Figure 11. Variation of field intensity in the channel at different bias voltages.

At a constant DC bias voltage, the electric field inside the microchannel plate can be approximated as a uniform electric field, with the electric field direction inside the channel parallel to the channel axis [28]. When the electrode penetration depth at both ends of the channel is a constant value, the higher the applied voltage, the higher the field intensity and the higher the electric field force on the electrons inside the channel. The applied voltage increases from 700 V to 1000 V and the field intensity increases linearly at 200 μm. The larger the applied voltage, the greater the electric field force on the electrons in the channel, which will increase the number of electron collisions in the channel and, thus, increase the gain.

When the electron emission is a DC mode, the secondary electron multiplication behavior at different voltage were shown in Figure 12. The gain shows an obvious increase and, especially at 1000 V, there is a sudden increase. This contributes to the increase in the number of output electrons that generates a larger secondary electron yield. It is in agreement with the variations of field intensity shown in Figure 11. This contributes to the increase in the number of output electrons generating a larger secondary electron yield. From

Equation (1) [27], it is also verified that the gain increases with the increase in the applied bias voltage, but the other structural parameters are fixed. The most probable energy distribution trend of MCP output electrons is consistent and their peak energies are in the range of 2–7 eV. When the bias voltage is 750 V, the electron distribution is the most concentrated.
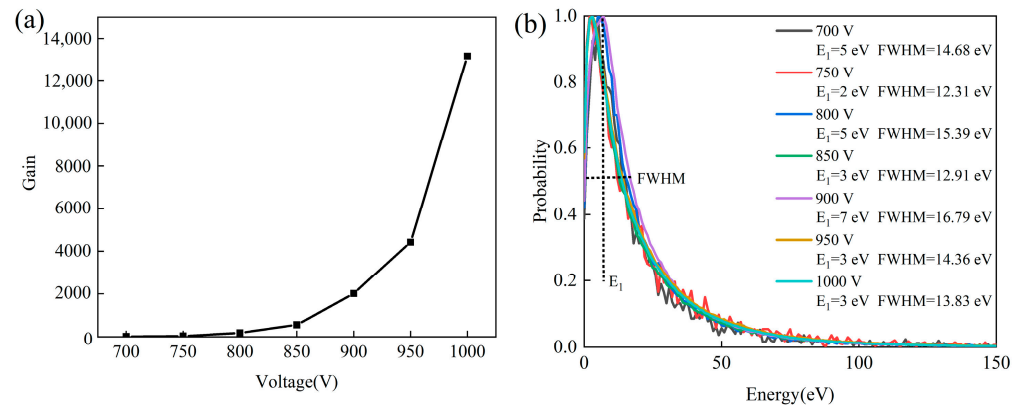

Figure 12. Effect of the applied voltage on secondary electron multiplication ($L/D = 39$, $\theta = 6^{\circ}$, $l_2 = 6$ μm): (**a**) Gain; (**b**) The most probable exit energy distribution.

4. Conclusions

In this paper, the effect of different structural parameters of the microchannel plate on its electron multiplication behavior and gain performance at DC electron emission modes was simulated based on FIT and the Monte Carlo method. The trajectories of multiplied electrons were also simulated. The trajectory generated by DC and by reported Gaussian pulse illustrate obvious differences. Due to the space charge saturation effect, the electric field force on the electrons in the channel decreases, the gain rise slows down, and the current density finally reaches saturation. Under the DC emission mode, the output–electrode penetration depth, bias angle, length-to-diameter ratio, and applied voltage are changed, respectively, and the simulation results show that the magnitude of electron gain increases with the increase in bias angle and applied voltage; the electron gain decreases with the increase in output–electrode penetration depth; the electron gain increases with the increase in length-to-diameter ratio under the normalized voltage, while there is a maximum value for length-to-diameter ratio from 15 to 50 under the same applied voltage. The most probable exit energy of electrons at the output of a single channel is simulated to concentrate on the range of 3–9 eV, which is the energy of the true secondary electron. The FWHM calculated from the simulations of the most probable exit energy influences the size of the luminous spot appearing on the fluorescent screen. Furthermore, the imaging qualities will be affected. The FWHM is relatively small for various preparation parameters and applied voltage, which is beneficial to reduce the crosstalk of secondary electrons signals output from so many fiber channel electron multipliers. However, both the highest gain values and the smallest FWHM could not usually be simultaneously achieved. In practice, the optimal producing parameters could be determined by the simulation results to balance them.

Author Contributions: Conceptualization, F.L. and Y.H.; simulation, D.J.; analysis, Y.S.; writing—original draft preparation, D.J.; writing—review and editing, F.L. and Y.H.; supervision, F.L.; project administration, P.J.; funding acquisition, Y.H. All authors have read and agreed to the published version of the manuscript.

Institutional Review Board Statement: Not applicable.

Informed Consent Statement: Not applicable.

Data Availability Statement: Data underlying the results presented in this paper are not publicly available.

Conflicts of Interest: The authors declare no conflict of interest.

References

1. Martindale, A.; Lapington, J.S.; Fraser, G.W. Photon counting with small pore microchannel plates. *Nucl. Instrum. Methods Phys. Res. Sect. A* **2007**, *573*, 111–114. [CrossRef]
2. Lu, N.; Yang, Y.; Lv, J.; Pan, J.; Liang, M.; Wang, X.; Li, Y. Neutron Detector Design Based on ALD Coated MCP. *Phys. Procedia* **2012**, *26*, 61–69. [CrossRef]
3. Zhang, Y.H.; Litvinov, Y.A.; Uesaka, T.; Xu, H.S. Storage ring mass spectrometry for nuclear structure and astrophysics research. *Phys. Scr.* **2016**, *91*, 073002. [CrossRef]
4. Fraser, G.W.; Pearson, J.F. The direct detection of thermal neutrons by imaging microchannel-plate detectors. *Nucl. Instrum. Methods Phys. Res. Sect. A.* **1990**, *293*, 569–574. [CrossRef]
5. Michalet, X.; Siegmund, O.H.W.; Vallerga, J.V.; Jelinsky, P.; Millaud, J.E.; Weiss, S. Photon-counting H33D detector for biological fluorescence imaging. *Nucl. Instrum. Methods Phys. Res. Sect. A* **2006**, *567*, 133–136. [CrossRef]
6. Then, A.M.; Pantano, C.G. Formation and behavior of surface layers on electron emission glasses. *Non-Cryst. Solids* **1990**, *120*, 178–187. [CrossRef]
7. Huang, Y. Study on Electronic Properties and Conductive Mechanism of Microchannel Plates. Doctoral Dissertation, China Building Academy, Beijing, China, 2014.
8. Huang, Y.; Gu, Z.; Zhang, Y.; Liu, H.; Li, G. Nano-scale morphology on micro-channel plate lead silicate glass surface. *Chin. Ceram. Soc.* **2012**, *40*, 994–999. [CrossRef]
9. Chang, Z. The First Collision problem of a MCP gain model. *Acta. Photon. Sin.* **1995**, *24*, 318–323.
10. Chang, Z. Numeric Modelling of the MCP characteristics gated by ps pulse. *Acta. Photon. Sin.* **1995**, *24*, 347–353.
11. Cai, H.; Liu, J.; Niu, L.; Liao, H.; Zhou, J. Theoretical simulation of electron transit time and gain characteristics in microchannel plate. *HPLPB* **2009**, *21*, 1542–1546.
12. Wei, Y. Monte Carlo simulation and computation of single channel multiplying parameters in MCP. *J. Electron. Inf. Technol.* **1992**, *14*, 76–80.
13. Cai, H.; Liu, J.; Peng, X.; Niu, L.; Gu, L. Monte Carlo simulation for spatial resolution of MCP framing tube. *J. Shenzhen Univ. Sci. Eng.* **2012**, *29*, 85–90. [CrossRef]
14. Deng, P.; Lin, K.; Luo, Q.; Long, J.; Wang, D.; Lei, Y.; Huang, J.; Wang, Y.; Cai, H.; Liu, J.; et al. Study on gain uniformity of microchannel plate online first. *Laser Optoelectron. Progress* **2022**. *Accepted*.
15. Chen, L.; Wang, X.; Tian, J.; Zhao, T.; Liu, C.; Liu, H.; Wei, Y.; Sai, X.; Wang, X.; Sun, J.; et al. The Gain and Time Characteristics of Microchannel Plates in Various Channel Geometries. *IEEE Trans. Nucl. Sci.* **2017**, *64*, 1080–1086. [CrossRef]
16. Yang, Y.; Liu, S.; Zhao, T.; Yan, B.; Wang, P.; Yu, Y.; Lei, X.; Yang, L.; Wen, K.; Qi, M.; et al. Single electron counting using a dual MCP assembly. *Res. Sect.* **2016**, *830*, 438–443. [CrossRef]
17. Wu, M.; Kruschwitz, C.A.; Morgan, D.V.; Morgan, J. Monte Carlo simulations of microchannel plate detectors. I. Steady-state voltage bias results. *Rev. Sci. Instrum.* **2008**, *79*, 073104. [CrossRef]
18. Kruschwitz, C.A.; Wu, M.; Rochau, G.A. Monte Carlo simulations of microchannel plate detectors. II. Pulsed voltage results. *Rev. Sci. Instrum.* **2011**, *82*, 023102. [CrossRef]
19. Yao, W.; Liu, S.; Yan, B.; Zhao, G.; Dong, Y.; Wang, Z.; Zhu, K.; Zhang, B.; Wen, K.; Wang, Y. Study on Electron Source of Cold Cathode Plane and the Dynamic Range of Low Resistance MCP. *Infrared Technol.* **2022**, *44*, 310–314.
20. Furman, M.A.; Pivi, M.T. Probabilistic model for the simulation of secondary electron emission. *Phys. Rev. Accel. Beams* **2002**, *5*, 124404. [CrossRef]
21. Guo, L.; Xin, L.; Li, L.; Gou, Y.; Tian, J. Effects of secondary electron emission yield properties on gain and timing performance of ALD-coated MCP. *Nucl. Instrum. Methods Phys. Res. Sect. A Accel. Spectrometers Detect. Assoc. Equip.* **2021**, *1005*, 165369. [CrossRef]
22. Tskhakaya, D. The Particle-in-Cell Method. In *Computational Many-Particle Physics*; Fehske, H., Schneider, R., Weiße, A., Eds.; Springer: Berlin/Heidelberg, Germany, 2008; pp. 161–189.
23. Pan, J. Microchannel plates and its main characteristics. *J. Appl. Opt.* **2004**, *5*, 25–29.
24. Nobuyoshi, K. Output Electron Energy Distribution of Microchannel Plates: Effects of Output Electrode Structure. *Rev. Sci. Instrum.* **1986**, *57*, 354.
25. Nobuyoshi, K.; Masato, H. Absolute ion detection efficiencies of microchannel plates and funnel microchannel plates for multi-coincidence detection. *Rev. Sci. Instrum.* **1985**, *56*, 1329. [CrossRef]
26. Chen, L.; Wang, X.; Tian, J.; Liu, C.; Liu, H.; Chen, P.; Wei, Y.; Sai, X.; Sun, J.; Si, S.; et al. Simulation of the effects of coated material SEY property on output electron energy distribution and gain of microchannel plates. *Nucl. Instrum. Methods Phys. Res. Sect. A Accel. Spectrometers Detect. Assoc. Equip.* **2016**, *840*, 133–138. [CrossRef]
27. Rochau, G.A.; Bailey, J.E.; Chandler, G.A.; Nash, T.J.; Nielsen, D.S.; Dunham, G.S.; Garcia, O.F.; Joseph, N.R.; Keister, J.W.; Madlener, M.J. Energy dependent sensitivity of microchannel plate detectors. *Rev. Sci. Instrum.* **2006**, *77*, 667. [CrossRef]
28. Gatti, E.; Oba, K.; Rehak, P. Study of the Electric Field inside Microchannel Plate Multipliers. *IEEE Trans. Nucl. Sci.* **1982**, *30*, 461–468. [CrossRef]